

ARTICLE

Charge-State Assignment of Nanoscale Single-Electron Transistors from their Current-Voltage Characteristics

Received 00th January 20xx,
Accepted 00th January 20xx

DOI: 10.1039/x0xx00000x

Bart Limburg,^{†a,b} James O. Thomas,^{†a,b} Jakub K. Sowa,^b Kyle Willick,^c Jonathan Baugh,^c Erik M. Gauger,^d G. Andrew D. Briggs,^b Jan A. Mol,^{*b,e} and Harry L. Anderson^{*a}

The electronic and magnetic properties of single-molecule transistors depend critically on the molecular charge state. Charge transport in single-molecule transistors is characterized by Coulomb-blocked regions in which the charge state of the molecule is fixed and current is suppressed, separated by high-conductance, sequential-tunneling regions. It is often difficult to assign the charge state of the molecular species in each Coulomb-blocked region due to variability in the work-function of the electrodes. In this work, we provide a simple and fast method to assign the charge state of the molecular species in the Coulomb-blocked regions based on signatures of electron-phonon coupling together with the Pauli-exclusion principle, simply by observing the asymmetry in the current in high-conductance regions of the stability diagram. We demonstrate that charge-state assignments determined in this way are consistent with those obtained from measurements of Zeeman splittings. Our method is applicable at 77 K, in contrast to magnetic-field-dependent measurements, which generally require low temperatures (below 4 K). Due to the ubiquity of electron-phonon coupling in molecular junctions, we expect this method to be widely applicable to single-electron transistors based on single molecules and graphene quantum dots. The correct assignment of charge states allows researchers to better understand the fundamental charge-transport properties of single-molecule transistors.

Introduction

Single-molecule transistors (SMTs) provide a platform for studying the magnetic and electronic properties of single molecules. Not only do the charge transport properties of SMTs depend on the charge state of the molecule, but a number of the interesting phenomena, such as magnetic anisotropy or quantum interference, are impossible to interpret correctly if the charge and spin state are unknown.¹⁻³ One cannot assume that the molecule will be in a neutral state at zero gate voltage, because charge transfer can occur between a redox-active molecule and the electrodes (as demonstrated below).⁴ Furthermore, the exact gate potentials at which molecular redox processes occur differ from device-to-device (and can even change in the same device over time), due to differences in the local electrostatic environment and

work-function of the electrodes, which makes it difficult to determine the charge state of the molecule at a given gate voltage.² The conventional methods of determining the molecular charge state, such as measuring the Zeeman effect,⁵⁻⁷ the Kondo effect,^{4, 8-11} or the presence of characteristic molecular features,^{3, 12} usually require precise, time-consuming measurements at low temperatures (*e.g.* 4 K and below, so that the energies of interactions, such as the Zeeman splitting, are less than the thermal energy $k_B T$). In this work, we show that a charge stability diagram, *i.e.*, a 2D plot of the current (I_b) as a function of bias voltage (V_b) and gate voltage (V_g), of a weakly coupled molecular species contains sufficient information to assign its charge state at temperatures as high as 77 K.

We fabricate three-terminal, single-electron transistor (SET) devices using graphene as the source and drain electrode material; see Figure 1a for the device architecture. Graphene-based devices are ideal for studying electron transport in a SET. The two-dimensional nature of graphene allows unrivalled electrostatic gate control while strong sp^2 carbon-carbon bonds are stable under the high electric fields across the junction.¹²⁻¹⁵ Feedback-controlled electroburning can be used to fabricate nanometer-separated graphene source and drain electrodes, termed graphene nanogaps (GNGs).^{16, 17} Electroburnt GNGs can be functionalized with molecules to generate SMTs.^{12-15, 18-20} The presence of small fragments of graphene (*i.e.* graphene quantum dots, GQDs) in the GNG can also generate a SET with a molecular character, even though the molecular structure of the GQD is unknown.^{21, 22}

^a Department of Chemistry, University of Oxford, Chemistry Research Laboratory, Oxford OX1 3TA, UK. Email: harry.anderson@chem.ox.ac.uk

^b Department of Materials, University of Oxford, Parks Road, Oxford OX1 3PH, UK. Email: jan.mol@materials.ox.ac.uk

^c Institute for Quantum Computing, University of Waterloo, Waterloo, ON N2L 3G1, Canada

^d SUPA, Institute of Photonics and Quantum Sciences, Heriot-Watt University, Edinburgh, EH14 4AS, UK

^e Department of Physics, Queen Mary University, London, E1 4NS, UK

[†] These authors contributed equally.

Electronic Supplementary Information (ESI) available: the procedure for extracting the rate constants, a charge stability diagram of the GQD device measured at 77 K, statistical factors for molecules with orbital degeneracy, and stability diagrams recorded of porphyrin single molecule transistors at 77 K. See DOI: 10.1039/x0xx00000x

It is typically found that a molecular species in a GNG is weakly coupled to the source/drain electrodes, *i.e.*, $E_c > \Gamma$, $k_B T$ where E_c is the charging energy of the molecule, Γ is the molecule-electrode coupling, and $k_B T$ is thermal energy. This leads to current suppression (Coulomb blockade) when the molecular energy levels are outside the bias voltage window (*i.e.*, the energy gap between the source and drain electrodes). When the energy of a molecular level is tuned using the gate electrode such that it falls within the bias window, sequential tunneling occurs: electrons tunnel from one electrode onto the molecule, and then tunnel off the molecule to the other electrode. Therefore a charge stability diagram of a weakly coupled molecular junction exhibits regions of high current where sequential electron transfer occurs, and diamond-shaped regions (Coulomb diamonds) where the current is suppressed, see Figure 1b for example. Within a Coulomb diamond (white in Figure 1b), the charge on the molecular species is fixed. Traversing through a sequential tunneling region (red or blue in Figure 1b) to the next Coulomb diamond by changing the gate potential changes the charge on the molecule by one; thus the sequential tunneling regions can be identified as charge transitions.^{23, 24} During sequential tunneling, an electron tunnels onto a molecule and resides there for some time (determined by the molecule-electrode coupling) before it tunnels off. As the equilibrium geometry of a molecule changes with oxidation state, the nuclear positions oscillate during the electron transport. Consequently, electron-phonon coupling is an important contributor to the conductance of single-molecule transistors.^{5, 12, 13, 25} In this article, we consider SETs to be molecular in nature when: 1) the energy spacing between successive charge states is much larger than thermal energy, $k_B T$, and 2) charging of the molecular species causes changes in its geometry, leading to large electron-phonon coupling in the sequential tunneling region.

The magnitude of the shift in the potentials of the experimentally accessible molecular levels is determined by a trade-off between the breakdown voltage of the gate dielectric and the gate coupling, and is typically limited to around 1 eV.² In SETs constructed from lithographically defined semiconductor quantum dots, the energy difference between successive electronic levels is small (a few meV) due to the larger size of the quantum dots, resulting in the observation of many small Coulomb diamonds. However, for SMTs, the gaps between successive energy levels are much larger (even for large π -conjugated molecules, HOMO–LUMO gaps are typically 1.5–2.0 eV) and as a result typically only 1 or 2 charge transitions, and therefore molecular oxidation states, are observed within the experimental window.² If we want to understand the charge transport properties of the SET then it is necessary to assign these charge transitions. A simple method for doing so is outlined below.

Results and discussion

A GQD device was fabricated in a previously reported SET architecture (device A), see Figure 1a.^{14, 20} The device was

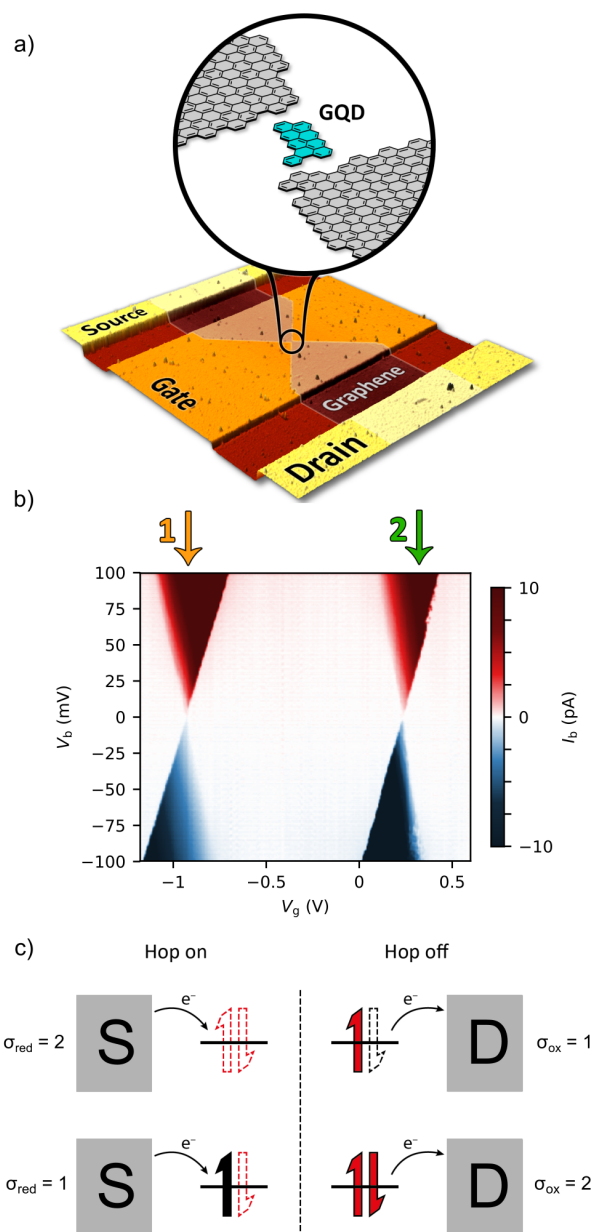


Figure 1 a) False-color AFM image ($8.2 \times 7.5 \mu\text{m}$) of the device architecture and artistic depiction of the GQD (the exact chemical structure is unknown). The gate electrode (orange) and substrate (Si/SiO₂, red) are separated from the graphene by a 10 nm layer of HfO₂. b) Charge stability diagram of device A at 16 mK, showing two sequential tunneling resonance regions labeled 1 and 2. c) Illustration of the origin of the statistical factors for a 0-1 transition, (upper panel) or 1-2 transition (lower panel), the red arrows represent the electrons and holes that can be involved in electron transfer.

cooled to 16 mK in a dilution refrigerator, and a charge stability diagram was recorded (Figure 1b). The diagram shows two regions of high conductance (resonance 1 and 2) and Coulomb-blocked regions surrounding them, indicating weak coupling to the electrodes. The current within the sequential tunneling region can be described using a rate-equation model:^{26, 27}

$$I_b = |e| \frac{\gamma_{red}^S \gamma_{ox}^D - \gamma_{red}^D \gamma_{ox}^S}{\gamma_{red}^S + \gamma_{ox}^D + \gamma_{red}^D + \gamma_{ox}^S} \quad (1)$$

Here, e is the elementary charge and γ_{red}^l and γ_{ox}^l are the rates of the reduction and oxidation process, respectively; the superscript indicates at which electrode the process occurs ($l = S$ or D for source or drain, respectively). The rates for each electrode are defined as follows.

$$\gamma_{red}^l = \int f(\epsilon) k_{red}^l(\epsilon) d\epsilon \quad (2)$$

$$\gamma_{ox}^l = \int (1 - f(\epsilon)) k_{ox}^l(\epsilon) d\epsilon \quad (3)$$

In equations (2) & (3), $f(\epsilon)$ is the Fermi-Dirac distribution, $k_{red}^l(\epsilon)$ and $k_{ox}^l(\epsilon)$ are the energy-dependent rate constants for reduction and oxidation, respectively at electrode l . The rate constants k_{red}^l and k_{ox}^l further depend on the electronic coupling to the source or drain electrode, Γ_S or Γ_D , and a statistical factor, σ , determined by the degeneracy of the molecular level involved in electron transfer. We can therefore rewrite the electron transfer rates in terms of density of states functions $\hat{k}_{red/ox}$ as:²⁶

$$\gamma_{red}^l = \frac{\Gamma_l \sigma_{red}}{\pi} \int f_l(\epsilon) \hat{k}_{red}(\epsilon) d\epsilon \quad (4)$$

$$\gamma_{ox}^l = \frac{\Gamma_l \sigma_{ox}}{\pi} \int [1 - f_l(\epsilon)] \hat{k}_{ox}(\epsilon) d\epsilon \quad (5)$$

For most molecular species, the frontier orbitals are merely spin degenerate (*i.e.* spin up and spin down electrons within the orbital are degenerate, and no orbital degeneracy is present). Orbital degeneracy in the frontier orbitals of

molecular species occurs only when the molecule is of high symmetry, which we do not expect to be the case for the GQD we measure. Therefore we expect $\sigma = 2$ for the rate of either the reduction (*i.e.* an electron hopping onto the molecule from an electrode) or oxidation (*i.e.* an electron hopping from the molecule to an electrode) process. The origin of the statistical factor is demonstrated in Figure 1c, and outlined in the following paragraph.

If the sequential tunneling that we observe involves an electron hopping onto the molecule into the LUMO, and hopping off the molecule from a singly occupied molecular orbital (SOMO) then electrons of either spin can tunnel into the LUMO, but only the electron in the SOMO can tunnel off. We term this a 0-1 transition, where the numbers refer to the occupancy of the transporting orbital either side of the charge transition (from lower to higher V_g). For a molecule that is closed shell when it is neutral, and does not display orbital degeneracy, this is simply a singlet-doublet transition. Conversely, if the transition involves an electron hopping into a SOMO and then from a doubly occupied orbital, then only electrons with a spin opposite to that of the electron on the molecule can tunnel onto molecule, but either of the two electrons on the molecule can tunnel off. We term this a 1-2 transition (or a doublet-singlet transition for the simplest case mentioned above). Therefore, we expect $\sigma_{red} = 2$ and $\sigma_{ox} = 1$ in the case of a 0-1 transition, and conversely we expect

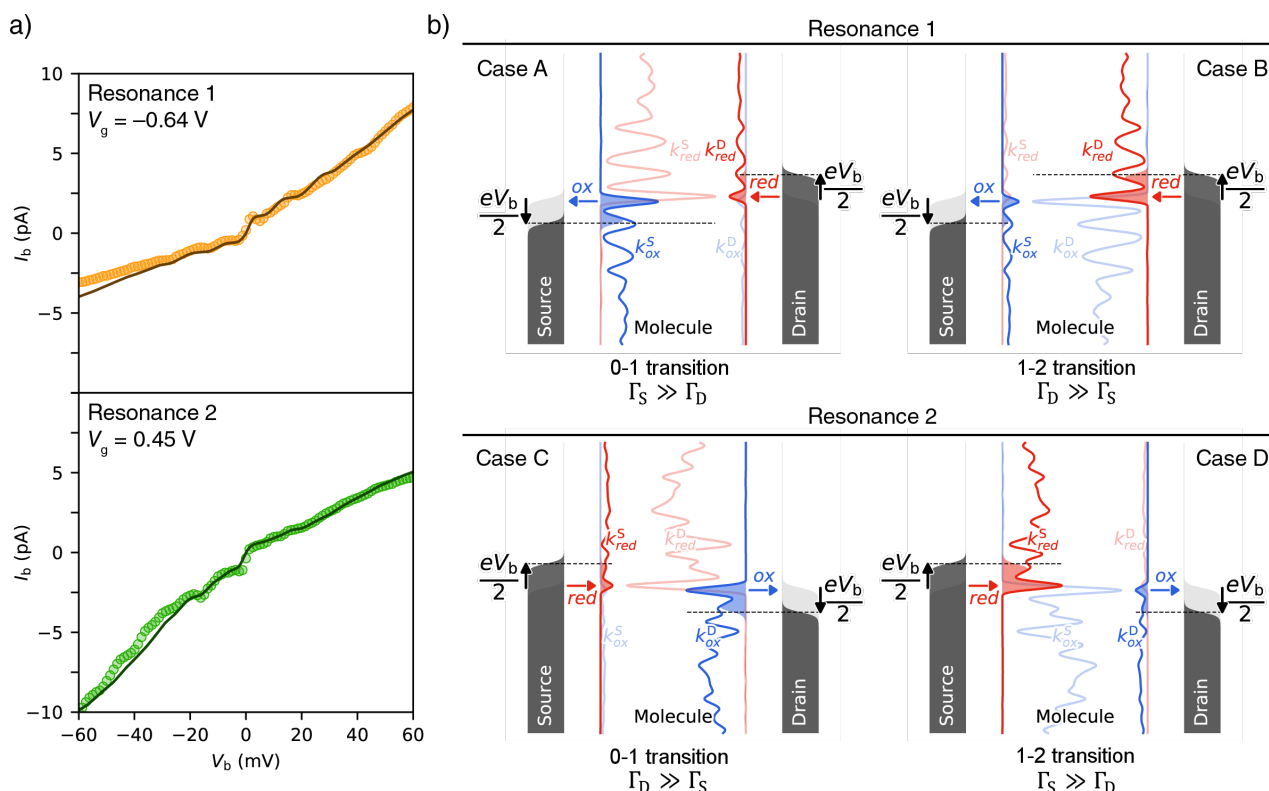


Figure 2. a) Resonant IV traces of the two sequential tunneling regions and reconstructed IV traces from extracted rate constants for device A resonance 1 and 2. Note the resonances (at $V_g = -0.64$ V and 0.45 V) have shifted slightly compared to Figure 1b. b) Four schematic overviews of the rate constants at either electrode. Each resonant IV trace can be described by two different combinations of electronic coupling and statistical factor. Together, the two resonances provide the four possible combinations of electronic coupling and statistical factors, shown as case A, B, C and D. The Fermi-Dirac distributions are shown as grey areas, and the rates γ are shown as the coloured areas under the rate constant curves. The bias voltage (V_b) is set to an arbitrary value in order to best visualize the rates.

$\sigma_{red} = 1$ and $\sigma_{ox} = 2$ in the case of a 1-2 transition.

We can extract $k_{red}(\epsilon)$ and $k_{ox}(\epsilon)$ from an IV trace measured on-resonance (*i.e.* a plot of I_b vs. V_b at the value of V_g corresponding to a charge transition) as illustrated in Figure 2a,b (for full details of the procedure, see ESI). From the rate constants, we can reconstruct the IV trace using equation 1. Figure 2a shows that the model describes the experimental data well. However, as we do not *a priori* know the charge state of the QGD, each IV trace can be reconstructed from two sets of parameters (see Figure 2b case A [0-1 transition] and B [1-2 transition] for resonance 1, or case C [1-2 transition] and D [0-1 transition] for resonance 2). Electron-phonon coupling results in $k_{red}^l(\epsilon)$ and $k_{ox}^l(\epsilon)$ covering a broad energy range, causing a gradual increase in the current as a function of bias voltage.²⁰ The shape of $k_{red}^l(\epsilon)$ (or indeed $k_{ox}^l(\epsilon)$) is the same on both electrodes ($l = S$ or D), but their magnitude is scaled by the electronic coupling Γ_S vs. Γ_D (we assume a constant density of states in the leads throughout, *i.e.*, the wide-band approximation). This causes an asymmetry in the rates at either electrode, and one of the electrodes to limit the current.²⁸ The shape of $k_{red}^l(\epsilon)$ is mirrored around the molecular level to obtain $k_{ox}^l(\epsilon)$, but its magnitude differs by the statistical factor, σ , originating from the spin degeneracy of the transporting orbital [*i.e.*, $\sigma_{red}k_{red}^l(\epsilon) = \sigma_{ox}k_{ox}^l(-\epsilon)$, where $\epsilon = 0$ is the molecular level], as discussed above. The combination of asymmetric coupling to the leads (Γ_S vs. Γ_D) and the statistical factor (σ_{red} vs. σ_{ox}) causes the four rate constants to have different magnitudes.

For resonance 1 (Figure 2), the resonant IV -trace can be described by two combinations of the statistical factors σ_{red} and σ_{ox} , and electrode couplings Γ_S and Γ_D . In order to extract the rate constants, we must deconvolute these factors, which can be done by fixing the statistical factors. If we fix them to be $\sigma_{red} = 2$ and $\sigma_{ox} = 1$, (case A, a 0-1 transition) and we fit the resonant IV trace we find that the current is limited by rates at the drain interface ($\Gamma_S \gg \Gamma_D$). Therefore, for case A, at positive V_b (as displayed in Figure 2b) the rate is limited by γ_{red}^D , at negative V_b the rate is limited by γ_{ox}^D . Due to the statistical factors ($\gamma_{red}^D = 2 \times \gamma_{ox}^D$) the magnitude of current at positive bias voltage is twice that at negative bias voltage. For case B we fix the statistical factors to be $\sigma_{red} = 1$ and $\sigma_{ox} = 2$ (a 1-2 transition), now if we fit the resonant IV trace we find $\Gamma_D \gg \Gamma_S$, *i.e.*, the current is limited at the source. Therefore, for case B at positive V_b (Figure 2b) the rate is limited by γ_{ox}^S , and at negative V_b the rate is limited by γ_{red}^S . Due to the statistical

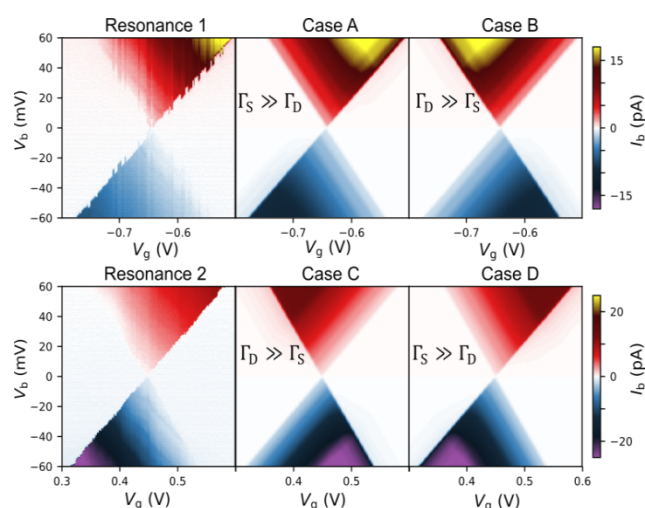


Figure 3. Charge stability diagrams of resonance regions 1 and 2 at 16 mK of device A (left panels), and reconstructed stability diagrams (center and right panels) for the corresponding cases in Figure 1Figure 2. In each diagram, the highest absolute current is indicated by the yellow (positive current) or purple (negative current) triangular region. The charge degeneracy points shift slightly between successive measurements (*i.e.*, compared to Error! Reference source not found.), due to filling and emptying of charge traps in the dielectric.

factors $\gamma_{ox}^S = 2 \times \gamma_{red}^S$, again we observe that the magnitude of the current at positive bias voltage is twice that at negative bias voltage. We stress that both case A and case B describe the current equally well, and no differentiation between the two can be made from only the resonant IV trace. In contrast, for resonance 2 either the current is limited by rates at the drain ($\Gamma_D \gg \Gamma_S$) and the transition is 0-1 (case C, $\sigma_{red} = 2$ and $\sigma_{ox} = 1$), or the current is limited at the drain ($\Gamma_S \gg \Gamma_D$), and the transition is 1-2 (case D, $\sigma_{red} = 1$ and $\sigma_{ox} = 2$). It is possible to go through the same logic as outlined for Resonance 1 to show that both cases give rise to a magnitude of current at negative bias voltage that is twice that at positive bias. We note that for two consecutive resonances of the same species, the four possible cases complement each other, *i.e.*, they are the only four possible combinations of the electronic coupling asymmetry and the statistical factors for electron transport through a spin-degenerate level. Experimentally, the coupling to electrodes is not controllable and almost all graphene-based devices are observed to exhibit a current that is limited by one electrode.^{14, 20} However, from a resonant IV trace, we cannot tell which of the two interfaces is limiting the current.

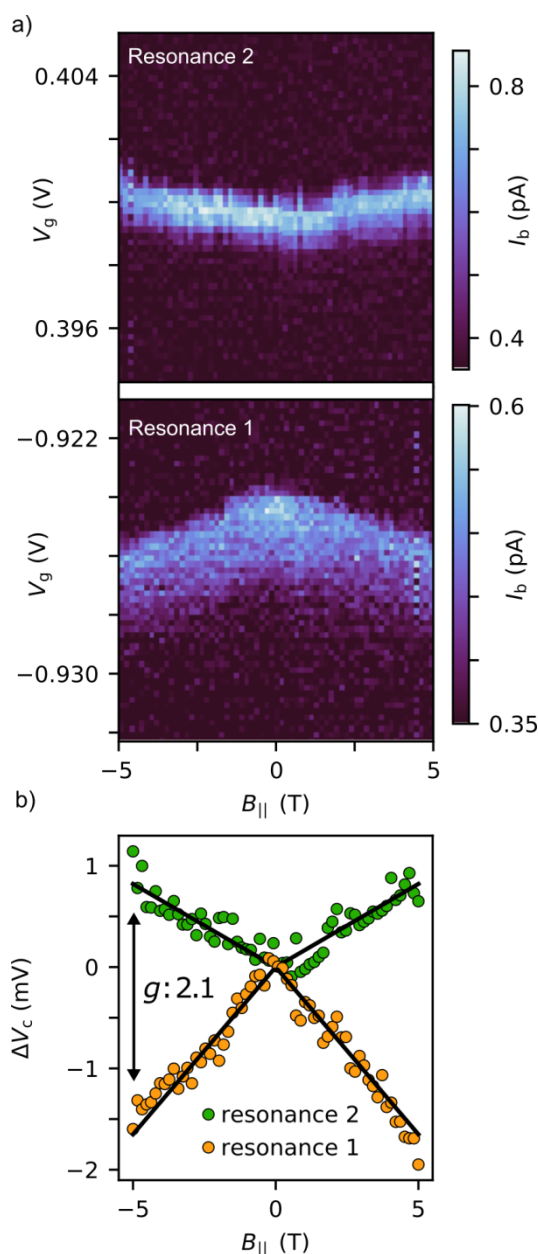


Figure 4 a) Current as a function of gate voltage and magnetic field measured at a bias voltage of 1 mV for device A resonance 1 and 2. b) Shift of peak maximum for both resonances from their initial position at $V_g = 0$ as a function of magnetic field. The Zeeman splitting between the two levels has a g -factor of 2.1.

Even though an on-resonance IV trace does not allow us to distinguish case A from B, or case C from D, the resulting stability diagrams are not symmetric with respect to gate voltage. Figure 3 shows the experimental stability diagrams for resonance 1 and 2, and stability diagrams reconstructed from the rate constants extracted from the IV traces of resonance 1 to cases A and B and resonance 2 to cases C and D. Evidently, resonance 1 is described by case A, and not case B, whereas resonance 2 is described by case D and not C. Therefore, the GQD has a singly occupied orbital at zero gate voltage, in the central Coulomb-blocked region, and the GQD is more strongly coupled to the source, $\Gamma_S \gg \Gamma_D$. The origin of asymmetry with

respect to the gate voltage is outlined for case A below (the same logic can be applied to cases B, C, and D). For case A, at a fixed positive V_b (e.g. Figure 2b) the current is limited by γ_{red}^D , as explained previously. This depends on the overlap of k_{red}^D with filled states in the leads (equation 2). As V_g is increased, the energy level, and consequently $k_{red/ox}^L$, are stabilized and this increases the overlap of k_{red}^D with filled lead states, thereby increasing the magnitude of the current with increasing V_g . Conversely at a fixed negative V_b , the rate is limited by γ_{ox}^D , which depends on the overlap of k_{ox}^D with empty states in the electrodes (equation 3). Again, as V_g is increased, $k_{red/ox}^L$ are stabilized and this *decreases* the overlap of k_{ox}^D with empty electrode states and therefore current decreases with increasing V_g . Whilst the fitting procedure is trivial in itself, it leads to an even simpler rule for assigning the charge state: the part of the sequential tunneling region where the absolute current is highest is on the side of the singly occupied orbital state (the yellow and purple triangles in Figure 3). This method is not hindered by thermal broadening, because it does not rely on precise measurement of the current, so the same conclusion can be obtained from a charge stability diagram at 77 K (see ESI) in very short data-acquisition times (10 minutes).

To unambiguously prove that the assignment of the charge state of the GQD deduced above for device A is correct, we measured the gate traces (a measure of I_b vs. V_g) of the resonant peaks at low bias voltage (1 mV) as a function of a magnetic field. The magnetic field was applied parallel to the plane of the graphene, approximately in the direction of the current. Figure 4a shows the current response as a function of gate voltage and magnetic field. Resonance 1 moves to more negative gate voltage, whereas resonance 2 moves to more positive gate voltage upon increasing the magnitude of the magnetic field. Each vertical slice in Figure 4a was fitted to a Lorentzian function and the maximum was plotted as a function of magnetic field in Figure 4b, which shows the linear dependence of both resonances on magnetic field. In a parallel magnetic field, the contribution of orbital angular momentum from the graphene is expected to be negligible, and only the Zeeman effect contributes to the splitting of spin-degenerate levels. A g -factor of 2.1 was obtained as the split between both levels of the GQD. This indicates that the split occurs due to a single unpaired electron, therefore confirming our assumption that the level is merely spin-degenerate.²⁹ Zeeman splitting of an unoccupied level creates two (spin-up and spin-down) unoccupied levels and electrons can tunnel through the spin state that is lower in energy, therefore for a 0-1 transition the resonance will move to lower gate voltages. Conversely Zeeman splitting of a singly occupied level creates one spin state at lower energy that will be occupied and one spin state at higher energy that will be unoccupied and only this level can be tunneled through, and therefore for a 1-2 transition the resonance will move to higher gate voltages. The assignments in Figure 3 match these predictions, and the fact that the resonances move away from each other confirms that in the region between the resonance 1 and 2 the highest-energy occupied orbital contains a single unpaired electron.

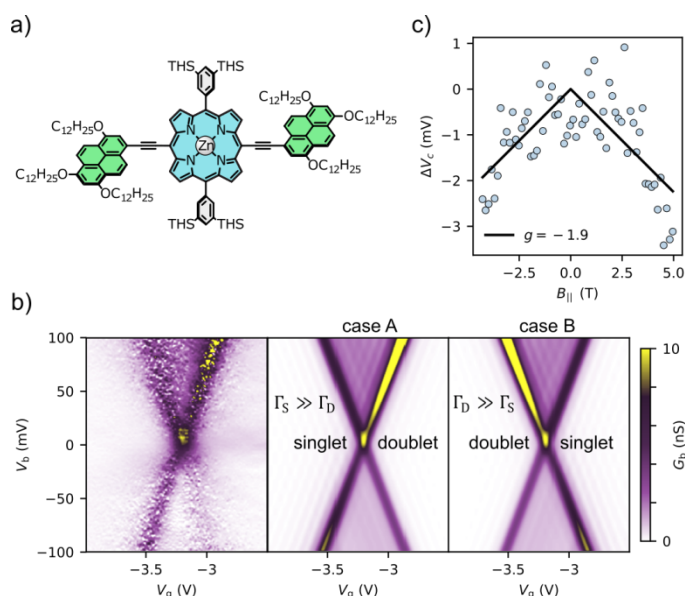


Figure 5 a) Structure of the molecule used in device B, bearing a redox-active central core (blue), solubilizing groups (grey, THS = trihexylsilyl), and graphene anchor groups (green). b) Differential conductance (G_b) diagram of a SMT containing a porphyrin molecule at 29 K (device B), and corresponding reconstructed charge stability diagrams for case A and B. For this device, the resonance IV trace was fitted according to reference 20 to obtain the rate constants. The yellow regions indicate the highest conductance. c) Magnetic field dependence of the charge neutrality point.

In addition to the QGD device A, we performed the same analysis on a porphyrin-based SMT (device B). The molecular structure of the species deposited from solution onto a GNG is depicted in Figure 5a, we showed recently that this molecular design leads to a high junction formation probability.¹⁴ A charge stability diagram reveals a clear sequential tunneling region (Figure 5b). Due to a high electronic coupling to the electrodes, the instability of the device, and the relatively weak electron-phonon coupling, the initial assignment based on the charge stability diagram was ambiguous. However, a differential conductance diagram (*i.e.*, the derivative of the charge stability diagram; a plot of the conductance, $G_b = dI_b/dV_b$ vs. V_b and V_g) allowed a clear assignment of the charge transition. The electronic structure of the molecule from density functional theory (DFT) calculations (see ESI) confirms that the frontier orbitals of the molecule are merely spin-degenerate. The charge transition was assigned to case A (Figure 5a), a 0-1 transition with $\Gamma_D \gg \Gamma_S$. We tested our assignment again by analyzing the magnetic field dependence of the resonance peak. The shift of the resonance point towards more negative gate voltage upon increasing the magnetic field (Figure 5c) is confirmation that this is a 0-1 transition (specifically singlet to doublet, as we know the molecule has no orbital degeneracy in the frontier orbitals, nor unpaired electrons in other orbitals). A g -factor of 1.9 was obtained, indicating an unpaired electron on the molecule at gate voltages more positive than the resonant point (a doublet state), in agreement with case A.

We have shown that the charge state of the molecule can be assigned simply by observing the highest-current corner of

the sequential tunneling region of its stability diagram. There are, however, various conditions that need to be satisfied:

(i) The molecule needs to be sufficiently redox active for the sequential tunneling region to be experimentally observable. In other words, the range of gate potentials must be sufficient to bring at least one of the frontier orbitals of the molecule in resonance with the Fermi levels of the source and drain electrodes.

(ii) The coupling to the electrodes needs to be sufficiently asymmetric (*i.e.*, $\Gamma_S \gg \Gamma_D$ or $\Gamma_D \gg \Gamma_S$). Experimentally, this condition is often satisfied, due to differences in the contacts between the electrodes and the molecule. We have previously shown that symmetric coupling is rare.²⁰

(iii) The assignment is simplest when the orbital that the electron transfers to/from is only spin degenerate. Although statistical factors can be calculated for different configurations in which both orbital degeneracy and spin degeneracy exist (see ESI), the assignment becomes cumbersome.³⁰ Experimentally, additional degeneracy in a SMT is unlikely as anchoring groups that functionalize redox-active molecules of interest tend to lift degeneracy in frontier orbitals, even if the unsubstituted molecule is highly symmetric, *e.g.* C_{60} .³¹

(iv) The rate constants should have non-zero values over a broad energy range to clearly show the asymmetry with respect to the gate. The molecular species should therefore have a different geometry in one charge state compared to the other, making electron-phonon coupling significant.

(v) Additional contributions to the tunneling current, such as excited states, must not mask the asymmetry arising from the spin statistics. In molecular systems electronic excited states generally occur at high energies (> 100 meV) and magnetic excited states at very low energies (< 1 meV). Therefore even if magnetic and electronic excited states occur on the same side of the resonant region for both polarities of bias voltage, they are unlikely to mask the asymmetric effect, and therefore they generally do not hinder the assignment. Another source of conductance lines in resonant transport regions are fluctuations in the density of states of the electrodes.³² As these lines do not lead to an overall increase in current they do not disturb the assignment. Indeed, in device A, not all the conductance lines (visible in Figure 3) run parallel to the edge of the diamond and the device appears to exhibit a mixture of density of state fluctuations and vibrationally excited states.

At first sight, the five conditions listed above might seem to restrict the method to a small number of devices. However, we expect that the conditions are met in most single-molecule transistors. To show this, we have checked the generality of our method for SMTs reported in the literature where the charge state was unambiguously determined. In many cases, the data show a region of highest current in the charge stability diagram, and we can verify our assignment technique. For example, the assignment based on molecular vibrations in a graphene-based SMT matches our assigned charge state.¹² The increase in off-resonant charge transport in a gold electro-migrated junction with an anthraquinone molecule matches the side of highest absolute current of the sequential region.³

Other gold-migrated junctions functionalized by ferrocene and tris(2,2'-bipyridine)iron(II) complexes have the highest current on the side which was assigned to have an unpaired electron by magnetic-field-dependent measurements.⁵ The presence of the Kondo effect in multiple electromigrated gold-molecular junctions also showed agreement with our assignment.^{4, 10, 11}

Finally, we checked a previous dataset of 26 single-molecule transistors that were made with porphyrin-based molecules that only differed by the anchoring group¹⁴ and were characterized by a charge stability diagram at 77 K, see ESI. From those 26 devices, 14 had a high enough data quality to perform further analysis, and 12 out of those 14 could be assigned. The devices that could not be assigned lacked the current asymmetry required for the method, or had a nearby transition which made assigning the state ambiguous. On the basis of our assignments 4/12 were found to have an unpaired electron at zero gate voltage. As the graphene was *p*-doped this suggests that for these devices the porphyrin has been oxidized upon adsorption onto the gap. Interestingly, three of the four devices with an unpaired electron at $V_g = 0$ belong to the molecule with the 1,3,6-tri(dodecoxy)pyrene (TDP) anchor group, which is the molecule with the lowest oxidation potential. The charge state assignment is important for understanding the charge transport behavior of these devices, and is obtained by a simple observation of the charge stability diagram recorded at 77 K. Furthermore, it has been demonstrated here that the naïve assumption that a molecular system within a junction is in a neutral charge state at zero gate voltage is not necessarily correct.

Conclusions

In summary, we demonstrate a simple method for assigning the charge state of a molecular transistor in a Coulomb blocked region based solely on the sequential tunneling regions in a charge stability diagram. The method can be used even at 77 K and works best for low-spin molecules that do not have orbital degeneracy in their frontier orbitals (or high-spin molecules if the electrons that are transported through the molecule do not pair existing unpaired electrons). It provides a quick and reliable way to assign the charge state without requiring precise magnetic-field-dependent data, or the presence of molecular features deemed to be specific to one charge state. This method provides, therefore, a simple way to gain a quantitative understanding of the behavior of molecular transistors.

Conflicts of interest

There are no conflicts to declare.

Acknowledgements

This work was supported by the EPSRC (grants EP/N017188/1 and EP/R029229/1). J.K.S. thanks the Clarendon Fund, Hertford College and EPSRC for financial support.

References

- 1 H. Y. Lam and N. Douglas, *Nanotechnology*, 2004, **15**, S517.
- 2 M. L. Perrin, E. Burzuri and H. S. J. van der Zant, *Chem. Soc. Rev.*, 2015, **44**, 902-919.
- 3 M. Koole, J. M. Thijssen, H. Valkenier, J. C. Hummelen and H. S. J. van der Zant, *Nano Lett.*, 2015, **15**, 5569-5573.
- 4 M. Koole, J. C. Hummelen and H. S. J. van der Zant, *Phys. Rev. B*, 2016, **94**, 165414.
- 5 N. P. de Leon, W. Liang, Q. Gu and H. Park, *Nano Lett.*, 2008, **8**, 2963-2967.
- 6 A. S. Zyazin, J. W. G. van den Berg, E. A. Osorio, H. S. J. van der Zant, N. P. Konstantinidis, M. Leijnse, M. R. Wegewijs, F. May, W. Hofstetter, C. Danieli and A. Cornia, *Nano Lett.*, 2010, **10**, 3307-3311.
- 7 E. Burzurí, Y. Yamamoto, M. Warnock, X. Zhong, K. Park, A. Cornia and H. S. J. van der Zant, *Nano Lett.*, 2014, **14**, 3191-3196.
- 8 W. Liang, M. P. Shores, M. Bockrath, J. R. Long and H. Park, *Nature*, 2002, **417**, 725.
- 9 L. H. Yu and D. Natelson, *Nano Lett.*, 2004, **4**, 79-83.
- 10 E. A. Osorio, T. Bjørnholm, J. M. Lehn, M. Ruben and H. S. J. van der Zant, *J. Phys.: Condens. Matter*, 2008, **20**, 374121.
- 11 C. B. Winkelmann, N. Roch, W. Wernsdorfer, V. Bouchiat and F. Balestro, *Nat. Phys.*, 2009, **5**, 876.
- 12 E. Burzurí, J. O. Island, R. Díaz-Torres, A. Fursina, A. González-Campo, O. Roubeau, S. J. Teat, N. Aliaga-Alcalde, E. Ruiz and H. S. J. van der Zant, *ACS Nano*, 2016, **10**, 2521-2527.
- 13 C. S. Lau, H. Sadeghi, G. Rogers, S. Sangtarash, P. Dallas, K. Porfyrakis, J. Warner, C. J. Lambert, G. A. D. Briggs and J. A. Mol, *Nano Lett.*, 2016, **16**, 170-176.
- 14 B. Limburg, J. O. Thomas, G. Holloway, H. Sadeghi, S. Sangtarash, I. C.-Y. Hou, J. Cremers, A. Narita, K. Müllen, C. J. Lambert, G. A. D. Briggs, J. A. Mol and H. L. Anderson, *Adv. Funct. Mater.*, 2018, **28**, 1803629.
- 15 J. A. Mol, C. S. Lau, W. J. M. Lewis, H. Sadeghi, C. Roche, A. Cnossen, J. H. Warner, C. J. Lambert, H. L. Anderson and G. A. D. Briggs, *Nanoscale*, 2015, **7**, 13181-13185.
- 16 C. S. Lau, J. A. Mol, J. H. Warner and G. A. D. Briggs, *Phys. Chem. Chem. Phys.*, 2014, **16**, 20398-20401.
- 17 F. Prins, A. Barreiro, J. W. Ruitenbergh, J. S. Seldenthuis, N. Aliaga-Alcalde, L. M. K. Vandersypen and H. S. J. van der Zant, *Nano Lett.*, 2011, **11**, 4607-4611.
- 18 P. Gehring, A. Harzheim, J. Spièce, Y. Sheng, G. Rogers, C. Evangeli, A. Mishra, B. J. Robinson, K. Porfyrakis, J. H. Warner, O. V. Kolosov, G. A. D. Briggs and J. A. Mol, *Nano Lett.*, 2017, **17**, 7055-7061.
- 19 P. Gehring, J. K. Sowa, J. Cremers, Q. Wu, H. Sadeghi, Y. Sheng, J. H. Warner, C. J. Lambert, G. A. D. Briggs and J. A. Mol, *ACS Nano*, 2017, **11**, 5325-5331.
- 20 J. O. Thomas, B. Limburg, J. K. Sowa, K. Willick, J. Baugh, G. A. D. Briggs, E. M. Gauger, H. L. Anderson and J. A. Mol, 2018, arXiv:1812.07562.
- 21 P. Gehring, H. Sadeghi, S. Sangtarash, C. S. Lau, J. Liu, A. Ardavan, J. H. Warner, C. J. Lambert, G. A. D. Briggs and J. A. Mol, *Nano Lett.*, 2016, **16**, 4210-4216.
- 22 A. Barreiro, H. S. J. van der Zant and L. M. K. Vandersypen, *Nano Lett.*, 2012, **12**, 6096-6100.
- 23 C. W. J. Beenakker, *Phys. Rev. B*, 1991, **44**, 1646-1656.
- 24 E. B. Foxman, P. L. McEuen, U. Meirav, N. S. Wingreen, Y. Meir, P. A. Belk, N. R. Belk, M. A. Kastner and S. J. Wind, *Phys. Rev. B*, 1993, **47**, 10020-10023.

- 25 M. Galperin, M. A. Ratner and A. Nitzan, *J. Phys.: Condens. Matter*, 2007, **19**, 103201.
- 26 J. K. Sowa, J. A. Mol, G. A. D. Briggs and E. M. Gauger, *J. Chem. Phys.*, 2018, **149**, 154112.
- 27 J. Zhang, A. M. Kuznetsov, I. G. Medvedev, Q. Chi, T. Albrecht, P. S. Hensen and J. Ulstrup, *Chem. Rev.*, 2008, **108**, 2737-2791
- 28 S. W. Wu, G. V. Nazin, X. Chen, X. H. Qiu and W. Ho, *Phys. Rev. Lett.*, 2004, **93**, 236802.
- 29 J. Güttinger, T. Frey, C. Stampfer, T. Ihn and K. Ensslin, *Phys. Rev. Lett.*, 2010, **105**, 116801.
- 30 R. Gaudenzi, J. de Bruijkere, D. Reta, I. d. P. R. Moreira, C. Rovira, J. Veciana, H. S. J. van der Zant and E. Burzurí, *ACS Nano*, 2017, **11**, 5879-5883.
- 31 P. Gehring, A. Harzheim, J. Spiece, Y. Sheng, G. Rogers, C. Evangelini, A. Mishra, B. J. Robinson, K. Porfyrakis, J. H. Warner, O. V. Kolosov, G. A. D. Briggs and J. A. Mol, *Nano Lett.*, 2017, **17**, 7055-7061.
- 32 P. Gehring, J. K. Sowa, J. Cremers, Q. Wu, H. Sadeghi, Y. Sheng, J. H. Warner, C. J. Lambert, G. A. D. Briggs and J. A. Mol, *ACS Nano*, 2017, **11**, 4739-4745.